CHAPTER 2

REVIEW OF HRR TEA CO_2 LASERS

This chapter briefly reviews the HRR TEA CO_2 lasers, excitation circuits, discharge kinetics, and glow-discharge formation. Factors and operating conditions affecting the HRR TEA CO_2 laser performance are also discussed. These may lead to better design and operation of a HRR TEA CO_2 laser system. Owing to the similar operation requirement of a HRR TEA CO_2 laser with respect to a normal TEA CO_2 laser, the theoretical considerations and mechanisms of the HRR laser are often referred to the latter.

2.1 REVIEW OF HRR TEA CO_2 LASERS AND EXCITATION CIRCUITS

This section describes various HRR TEA CO_2 lasers and their excitation circuits in terms of their applications, performance and uniqueness. Secondly, the operations of the excitation circuits and the preionizers are also provided. Lastly, the mechanical parts of the lasers such as their profiled electrodes, flow conditioners, heat exchangers and optical oscillators are also briefly reviewed.

2.1.1 Laser Performance

The many applications of TEA CO_2 lasers in optical ranging, tracking, remote sensing and material processing give rise to the development of the HRR TEA CO_2 laser. Most of the HRR TEA CO_2 lasers are small in size and produce a few hundred milli-joules of output energy per pulse and a few tens of watts of average output power. There are a few systems that produce

higher output energy per pulse and higher average power: Michon et al. [39] designed a HRR system with 8 kW of average output power at 520 pps (pulse per second or Hz) whereas Dumanchin et al. [40] reported a system with 20 J/pulse at 100 pps.

Most of the HRR TEA CO_2 lasers are operated at pulse repetition frequency (PRF) ranging from a few hundred Hz to 1 kHz, with two reported exceptions: (i) 5.5 kHz in burst mode of 10^4 pulses by Rickwood et al. [29] and (ii) 2 kHz by Tulip et al. [22]. The average input power for case (ii) was approximately 30 kW into a $2.5 \times 2.5 \times 60$ cm^3 active volume which is replenished at a gas flow velocity of 100 m/s.

Most HRR systems are designed to generate high peak power, ranging from a few hundred kW to more than 1 MW [40, 41], depending mainly on their discharge volume. Using a strong preionization and a fast discharge pumping pulse, high peak power from a small discharge volume has been obtained by increasing the CO_2 concentration, e.g. at >30% [42, 43], 60% [44], and >60% [45]. Some systems have been operated in Helium-free gas mixture, e.g. at 300-400 mbar of 1:1-CO_2:N_2 with 15 mbar H_2 [46], 1:1-CO_2:N_2 [43], 3:2-CO_2:N_2 [44], and 4:1-CO_2:N_2 [45].

A wavelength tunable HRR TEA CO_2 laser is needed for laser radar operation and other applications which include optical pumping of FIR (Far-Infrared) laser [47], isotope separation [47], photochemistry [30], frequency conversion [47], and spectroscopy. These tunable systems have been reported in the literatures [41, 42, 48, 49]. Normally, a 150 *l*/mm reflective diffraction grating as the back mirror of laser optical resonator is used for wavelength selection.

A miniature 10-mm^3 (50(L) × ~3(W) × 7(H) mm) active volume HRR TEA CO_2 laser has been reported by Dyer and Tait [43]. This laser produced a maximum average power of 6.3 W at 250 pps with an output peak power of 0.4 MW in TEM_{00} transverse mode. The gas mixture is 1:1-CO_2 :N_2 with 5% H_2 and the efficiency is ~4% with a 90% Ge output coupler.

Marchetti et al. [46] have reported a long-life sealed-off HRR TEA CO_2 laser in which a lifetime of more than 2×10^7 pulses has been achieved. This laser used hydrogen additive for reversing the discharge induced CO_2 dissociation process. A corona rod preionizer with minimal discharge induced CO_2 dissociation was also used. Stark et al. [44] had also developed a sealed-off system with a lifetime of more than 2×10^7 pulses. This system used the SnO_2-Pd catalyst to regenerate CO_2 from O_2 and CO with a 1% of CO additive. This system used the semiconductor preionizer instead of corona rod. With these long-life sealed-off systems, bulky gas supply and gas-handling facilities are removed, resulting in the ease of portability for laser radar applications.

The long-life sealed-off systems are also important when the expensive rare isotope $^{12}C^{18}O_2$, $^{13}C^{16}O_2$, and $^{13}C^{18}O_2$ gases are used. A high-power tunable HRR TEA-$^{13}C^{18}O_2$ laser was developed by Sugii et al. [49]. This system used the $^{15}N_2$ isotope instead of $^{14}N_2$ to increase the output energy by a factor of 2. The rare CO_2 isotope lasers are useful for optical radar and lidar applications because of reduced absorption by atmospheric CO_2 and enhanced capability for the detection and monitoring of pollutants. This laser produced an average output power of 25 W at 100 pps in multi-line and a maximum of 15 W of single-line operation at ~10.92 μm.

A sealed-off HRR CO_2 laser using an oxygen tolerant discharge scheme was developed by Dyer and Monk [50]. This is because the O_2, which is produced by discharge induced dissociation of CO_2 (§2.7), can lead to insufficient homogeneous glow discharge formation and/or discharge instabilities and arcs formation during the electrical discharge (§2.3.3). Therefore, the O_2 concentration usually governs system lifetime with a cutoff level of less than 1-2% [12, 46]. The Dyer and Monk's system used a combination of fast electrical pulsed discharge and near simultaneous UV-preionization to avoid arc formation [51] owing to decreasing photoelectron density via negative ion formation. An initial CO_2 bare gas mixture of

300:170:120:50 torr-He:N_2:CO:O_2, in which the total pressure is 640 torr (~850 mbar) and ~8% of O_2, was successfully operated with satisfactory discharge uniformity. With this gas mixture discharged at 30 pps, laser emission occurred after 2.7×10^3 shots of discharge as CO_2 was formed in the discharge and laser output stabilized after 1.8×10^4 shots.

Tulip et al. [22] developed a HRR TEA laser discharge using integrated preionization and switching. This system used a 10-stage Marx generator to pump the laser. The 10 triggered spark gaps were put inside the laser chamber and 5 cm downstream from the main discharge center. These spark gaps provided a strong and uniform UV-preionization in the discharge volume. Since the spark gaps operate in 1 atmospheric of 1:1:8-CO_2:N_2:He gas mixture, each spark gap has a 1-cm gap and was able to maintain a 6-kV voltage difference. The gas flow velocity across the main discharge is 100 m/s. With a total storage energy of 20 J, a maximum repetition of 2000 pps has been achieved. However, when the total storage energy was reduced to 3 J, the maximum repetition was 4000 pps. It was explained that the main discharge, which is upstream of the spark gaps, can affect the recovery strength of the spark gaps. In a continuous operation, this system has been operated at a maximum PRF of 2000 pps and an average input power of approximately 30 kW. No average output power was reported by the authors.

2.1.2 Excitation Circuits and Preionizers

(a) Excitation Circuits

In the pulsed excitation of a TEA CO_2 laser, two different circuits are normally used, (i) single-capacitor discharge (SCD) and (ii) LC inversion circuit [52, 53]. These are shown in Fig. 2.1. Generally, uniformly distributed peaking capacitors C_P [19, 20, 21, 22] are placed close to the laser channel for the initiation of a fast and uniform glow discharge. The total capacitance in C_P ranges from less than 1 nF [19, 29, 45, 46, 51] to a few nF [12, 20, 21, 22, 26, 27, 41, 44,

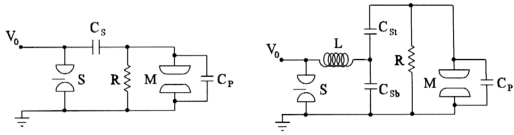

Single-capacitor discharge circuit **LC inversion circuit**

Fig. 2.1: Two common types of excitation circuits for TEA CO_2 laser (From Cridland and Howells [52], Houtman et al. [53]). The components are as follows: V_0 -- charging voltage of C_S, C_{Sb}, or C_{St}; S -- triggered spark gap; C_S -- storage capacitor; R -- bypass resistor; M -- laser channel; C_P -- peaking capacitor; L -- insertion inductor; C_{Sb} -- bottom storage capacitor; and C_{St} -- top storage capacitor. Normally $C_{Sb} = C_{St}$ in the LC inversion circuit.

49, 54, 55].

In the SCD circuit, when the switch S is closed at t = 0, the peaking capacitor is charged up by the storage capacitor C_S. The voltage across C_P before the laser channel M breaks down with neglected circuit resistances or losses is

$$V_P = -[V_0C_S/(C_S+C_P)](1-\text{Cos}\omega t) \tag{2.1}$$

where $\omega = [(C_S+C_P)/(L_{St}C_SC_P)]^{½}$ and L_{St} is the C_P-C_S-S loop inductance. Since $C_S > C_P$, only part of the charge of C_S is transferred to C_P and the maximum voltage, $V_P = -2V_0C_S/(C_S+C_P)$. After channel M breaks down, the energy stored in C_P is rapidly dumped into channel M followed by the remaining energy in C_S.

In the LC inversion circuit, the closure of switch S allows the storage capacitor C_{Sb} (Refer to Fig. 2.1) to discharge through the inductor L. The voltages across C_{Sb} (Eq. 2.2) and C_P (Eq. 2.3) before the channel M breaks down with large L are:

$$V_{Sb} = V_0[C_{eq}/(C_{eq}+C_P)]^{½}\text{Cos}\omega t \quad (2.2)$$

$$V_P = -V_0[C_{eq}/(C_{eq}+C_P)]^{½}(1-\text{Cos}\omega t) \quad (2.3)$$

where $\omega = (C_{Sb}L)^{-½}$ and $C_{eq} = C_{Sb}C_{St}/(C_{Sb}+C_{St})$. The maximum $V_P = V_{Sb} + V_{St} = -2V_0[C_{eq}/(C_{eq}+C_P)]^{½}$ if M does not break down. However, laser channel M normally breaks down for $-V_0 < V_P < -2V_0$ if $C_{eq} \gg C_P$.

A voltage multiplication at C_P with respect to the C_S-voltage normally occurs in SCD circuit if $C_P < C_S$. The LC inversion circuit also produces this voltage multiplication if a H.V. switch (spark gap or saturable inductor) is placed before the top electrode of the laser channel but this additional switch normally is not used in TEA CO_2 lasers. In CO_2 lasers, a lower E/N (the ratio of electric field across channel M to neutral particle density) will produce higher electrical excitation efficiency [52, 56] (§2.4). The SCD circuit is generally more efficient than [52] the LC inversion circuit. However, LC circuit is preferred for short-pulse glow discharge systems. In addition, the capacitor C_{Sb} in the LC circuit must have 100% reverse voltage capability for voltage multiplication.

In some systems, the LC sections are used in the SCD circuit to form a pulse forming network (PFN). This PFN circuit will produce long duration (~10 μs at 1-atm [57]) glow discharge [57, 58, 59]. Besides the above two simple excitation circuits, the spiker-sustainer circuit was also used [60, 61, 62]. The spiker is a high-voltage, low-energy, short-pulse circuit for initiating a uniform laser discharge whereas the sustainer is a switchless, low-voltage, high-energy, long-pulse circuit for sustaining the discharge. The sustainer voltage must be kept below the self-breakdown voltage of the laser channel. Since the amount of charge flowing through the H.V. switch is reduced, the lifetime of the switch is prolonged [25]. Besides, the sustainer provides a lower voltage to the laser channel which means that the excitation efficiency of this

circuit is higher.

The all-solid-state exciters (ASSE) [26, 27, 28, 62, 63], as mentioned in §1.2, are designed using SCRs, step-up pulse transformer, and saturable magnetic switches (MPC) to produce pulse voltage for the TEA CO_2 laser. This ASSE is also used as spiker in a spiker-sustainer system [62]. All the above mentioned circuits can be made to operate at high pulse repetition frequency (PRF) by replacing resistors with inductors and using capacitor charging unit.

(b) Preionizers

There are two common preionization schemes for TEA CO_2 laser: ultraviolet (UV) and electron-beam [64]. The former is the more widely used. The UV radiation can be generated by two means: spark/arc discharge and corona discharge. Fig. 2.2 shows some of these commonly used UV preionizers used in HRR TEA CO_2 lasers. These are sliding-spark array [42, 45, 51], capacitively ballasted parallel spark array [3, 50], corona wire [41, 46], semiconductor preionizer [29, 65], trigger wire [48], and cathode surface preionizer [12].

In the sliding-spark array, the arrangement of the spark electrodes can be arranged either in transverse or in linear configuration as shown in Fig. 2.2. The capacitive ballast parallel spark array is normally connected in parallel with the laser electrodes and the ballast capacitors are the peaking capacitors. The corona wire can be normally arranged in two ways: on the curved edges of the laser electrode or on the surface of the cathode. Machining of V-shaped grooves on cathode surface for insulated corona-wire seating is needed. The semiconductor preionizer is produced by the resistively distributed multiple-arc discharge to the edges of main anode. The trigger wire preionizer provides an inhomogeneous sheet glow discharge between the wire and the main electrode along their whole length. This sheet discharge provides dominantly the

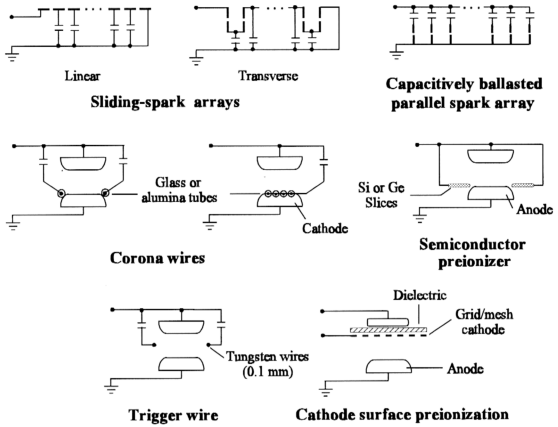

Fig. 2.2: Some common types of preionizer for HRR TEA CO_2 laser (From refs. [see text]).

photoemission on the cathode surface. The cathode surface preionizer forms a homogeneous glow discharge between the dielectric and grid (or mesh) cathode over their whole surface. This will provide a uniformly distributed electron source on the cathode surface.

A comparison among the sliding spark, corona wire, and semiconductor preionizers on the operation and output of TEA CO_2 lasers has been presented by Spiers et al [66]. The corona and semiconductor preionizers provided good pulse-to-pulse repeatability, but the semiconductor preionizer was the least efficient and the sliding spark was the most efficient. Nevertheless, the corona wire preionizer provided a good compromise between the two, with very homogeneous UV illumination.

For HRR operation with transverse gas flow, the presence of preionizer should produce minimal flow impedance. Furthermore, the upstream positioning of the preionizer can lead to premature arcing of the laser discharge [22] caused by previous spark-discharge by-products.

(c) Timing Between Preionizer and Main Discharge

All the preionizers can be operated either as part of the main discharge circuit or by a separate circuit. Preionizers, which are connected to the main discharge circuit, can be placed in different positions: between the H.V. switch and the main electrode or parallel with the main electrode. The time delay between the preionizer and main discharge is produced by using inductor, resistor, and/or capacitor which is either itself part of the circuit or as insertion elements.

The separate preionizer circuit is normally a single-capacitor discharge or charge-transfer (or capacitor-transfer, C-C) circuit which can be either driven by the same H.V. switch or by a separate H.V. switch. There were also circuits coupled by pulse transformers for operating the preionizer [12]. The time delay can be achieved by either external means or circuit elements means. The external time delay can be generated by electronic control or spark gap formative time-lag delay control [37, 38].

2.1.3 Laser Chamber Designs

Uniform field profiles are necessary in the laser electrodes as discussed by Ernst [8], Chang [7], Rogowski, or a pair of the profiled electrode and mesh grid [12]. The electrode materials are normally copper, brass, aluminium, stainless steel, nickel or nickel coated brass. Some electrodes were made of graphite [43] or carbon [22].

Continuous gas flow is often needed in the HRR TEA CO_2 laser. Several types of gas-

flow drivers have been used including parallel array of axial flow fans, tangential flow fans [44, 45, 50] and flex-vane blowers [30]. In addition, a gas flow ducting or guiding unit is also needed with either a shaped laser chamber as the gas flow duct [29, 42, 44] or internal ducting plates to guide the gas flow path. The laser chamber is normally in the form of stainless steel tube, perspex box, machined blocks of perspex or aluminium [29, 30], plastic plumbing parts and perspex plates [42], aluminium chamber, and Pyrex tube with metal end plates [50, 51]. The gas flow straightener and turbulence generator [12, 29, 42, 45, 48] were also used for improving flow uniformity and to increase the removal rate of the discharge products at the boundary layers above surfaces of electrodes [11]. The shock wave absorber, generated by the main discharge, was also used [30]. Heat exchanger using the water-cooled, multifinned copper pipes was placed either upstream or on both sides of the fan array. The water-cooled chamber wall [12] and water-cooled copper coils [44, 48, 50] were also used as the heat exchanger.

Laser optics usually consists of a concave total reflector of 2-20 m curvature and a plane partial reflector as output coupler. Stable resonator is often used although plane-plane resonator was also used [44]. The reflectivity of the output coupler, in the range of 60-90%, depends on the discharge length. Gold coated copper, BeCu, silver enhanced or uncoated copper mirrors are used as total reflectors and the substrate is normally copper or silicon. Two types of materials for the output coupler are generally used, i.e., germanium and zinc selenide. NaCl Brewster windows were also used, especially for wavelength tunable systems.

2.2 THE KINETIC PROCESSES IN TEA CO_2 LASER

The study of the kinetic processes in the TEA CO_2 laser is necessary because this leads to a better understanding of the parameters which affect output efficiency and pulse-shape of the CO_2 laser.

2.2.1 Vibrational States and Energy Levels

The CO_2 molecule is a linear, symmetric, triatomic molecule. It has an axis of symmetry along the nuclei and a perpendicular plane symmetry. The total degrees of freedom of a CO_2 molecule are nine (3 × number of atoms involves in the molecule). Therefore, a CO_2 molecule has three, two, and four normal coordinates or degrees of freedom for the translation, rotation and vibration motions, respectively. The corresponding vibrational motions are shown in Fig. 2.3. The symmetric and asymmetric stretch modes have frequencies f_1 and f_3 respectively and the doubly (or twofold) degenerate bending modes have frequency $f_{2a} = f_{2b} = f_2$ which vibrate in the plane mutually perpendicular to each other. This molecule can vibrate in more than one mode at the same time and can have more than one quantum of vibrational energy in each mode. Therefore, the degree of excitation of these individual modes are denoted by the quantum numbers of ($\mathbf{v}_1$, $\mathbf{v}_2^l$, $\mathbf{v}_3$) respectively, where $l = \mathbf{v}_2, \mathbf{v}_2 - 2, \ldots, 1$ or 0 due to $\mathbf{v}_2 = \mathbf{v}_{2a} + \mathbf{v}_{2b}$. Because of perturbation between degenerate levels $\mathbf{v}_2^l$, these energy levels split up and down as their energies decrease with l.

Fig. 2.3 also shows a few of the important low-lying vibrational energy levels of CO_2 and N_2 in their electronic ground states. On each vibrational level, including the ground state, there is a series of distributed rotational energy levels giving rise to a vibrational-rotational band. Because of the vibrational-rotational transitions between the upper (00^01) and lower {(10^00) and (02^00)} laser levels, the laser can be tuned to generate over 100 lines around 9.4 μm and 10.4 μm. The strong CO_2 laser transitions, which were designated as 10P(18), 10P(20), and 10P(22) of the 10.4-μm band [67, p. 19; 68, p. 59; 69, p. 28], are at about 10.6 μm. The closely located (10^00) and (02^00) levels are in Fermi resonance, which were first recognized by Fermi (1931) [68, p. 58]. The perturbation of energy of these levels results in one-level up-shifted and the other down-shifted from the actual positions. So, Amat and Pimbert (1965) [68, p. 58] suggested that a new nomenclature should be given as shown in the figure.

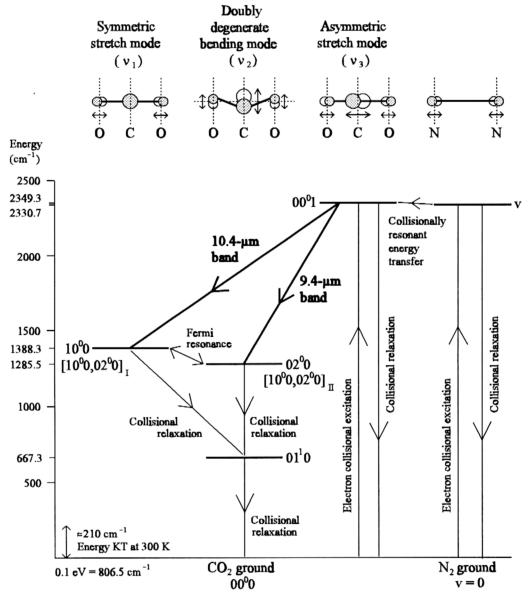

Fig. 2.3: Simplified vibrational energy-level diagram of CO_2 and N_2 for CO_2 laser (From Witteman [67, p. 65], Smith [69, p. 28], Tyte [71, p. 132]). The three normal modes of vibration of CO_2 are also included (From Witteman [67, p. 9]). Note that the rotational levels of each vibrational level (including ground states) are not shown.

2.2.2 Upper Laser Level Excitation Mechanism

At least three processes are known to be important in creating an upper laser-level population [70, pp. 224-226]:

I. Direct electron impact excitation

II. Electron impact pumping of N_2 and collisonally resonant energy transfer

III. Electron impact pumping of CO and collisionally resonant energy transfer

The electron-impact excitation cross sections (about $\leq 2 \times 10^{-16}$ cm^2) for the upper laser level (00^01) is larger than the lower laser level for electron energy in the range of ~0.8-2 eV. However, the cross sections for the lower laser level is larger when electron energies fall within ~2-10 eV [67, p. 151, 56]. This means that the population inversion is not created by this direct electron-impact excitation when electron energies fall within 2 to 5 eV (the average electron energies $\bar{u}_e$ for TEA CO_2 lasers are 2-4 eV [3]). The population inversion is actually achieved by the collisional relexation processes (§ 2.2.3).

The addition of N_2 into the CO_2 system results in an increase of the laser efficiency. It is due to the fact that the vibrationally excited levels, v = 1 to 6, of the N_2 molecules can near resonant energy transfer, through collision, to the ν_3 vibrational levels of CO_2 molecules with some excess energy coming from the translational energy (thermal energy kT). In fact, the vibrational energy transfer with smaller excess energy will lead to a larger probability. The excited levels of N_2 have very long lifetimes (many milliseconds) because its radiative decay is strictly forbidden (N_2 is a homonuclear diatomic molecule, and so has no dipole moment in the ground state) and it can only decay by collisions. When the interaction process with the CO_2 molecules during discharge involves a time scale of <1μs, the collisional excitation by excited N_2 is unimportant [3]. This is because the rate constant of the excited N_2 collisional energy transfer to CO_2 is 1.9×10^4 torr^{-1} s^{-1} at 300 K. Although the total effective cross section (~10^{-16}

cm^2) for vibrational excitation of N_2(v = 1-8) by electron impact falls in the electron energy range of 1.7-3.5 eV [67, p. 67], the collisional energy transfer to the CO_2 by the vibrationally excited N_2 is the main pumping mechanism in CO_2 laser.

The excited CO molecules can also, but less effective, transfer energy to the CO_2 molecules. This is because the (00^01) level of CO_2 is 206 cm^{-1} (KT = 210 cm^{-1} at 300 K and the temperature-rise after discharge is of the order of 75 °C [40]) higher than the vibrational level (ν = 1) of CO and the CO molecule has a dipole moment which can undergo spontaneous radiative decay. In fact, the excited $CO_2(00^01)$ can be depopulated by a large proportion of unexcited CO(ν = 0).

2.2.3 Laser Levels Relaxation Mechanism

There are two major processes in the relaxation mechanism [70, pp. 227-230]:

I. Radiative relaxation

II. Collisional relaxation

All the spontaneous radiative relaxations (radiative decays) are not significant processes in the CO_2 laser since their relaxation rates are orders of magnitude smaller than the collisional relaxation. This is due to the radiative decay coefficients (Einstein coefficients) for transitions in CO_2 laser are in the range of A = 0.2-2 s^{-1} [70, p. 227, 71, p. 143]. However, the radiative decay to the ground state of the upper laser level is strongly trapped by other unexcited CO_2 molecules, resulting in an effective A ≈ 10 s^{-1}. Also note that the upper laser level has a shorter radiative lifetime than the lower levels.

Since the collisional relaxation process is the dominant kinetic process in the CO_2 laser, this is the rate limiting the overall CO_2 laser system. In collisional relaxation processes, the relaxation rates within each degree of freedom (ν_1, ν_2, or ν_3) is much faster (few ns at high-

pressure [3]) than among the different vibrational modes (e.g., $\nu_3 \rightarrow \nu_2$, $\nu_2 \rightarrow \nu_1$). It is because the former is in the resonant energy sharing process. All the collisional processes can be reversible depending on the tendency of the sink direction. Similar to the vibrational energy transfer excitation case, the smaller excess energy will lead to a higher probability of the collisional relaxation.

The relaxation of the lower laser levels is limited by the relaxation of the (01^10) level to ground which involves 667 cm^{-1} energy transfer. The collisional relaxation of the upper laser level is the most important process, as it competes with stimulated emission for transferring molecules from upper to lower laser level. Table 2.1 shows the relaxations of ν_3 and ν_2 influenced by various gases. The overall rate for a particular relaxation in a complex mixture of gases can readily be calculated using the relationship [71, p.145]

$$K = \sum k_{CO_2,i}\, p_i \tag{2.4}$$

where $k_{CO_2,i}$ is the appropriate relaxation rate constant of the binary mixture of CO_2 and p_i is the partial pressure in torr of gas i. The relaxation time can be calculated as $\tau = 1/K$.

Although collisional relaxation rates are temperature dependent [70, p. 230] and increase with temperature generally [71, p. 147], this dependence is relatively unimportant for the short-pulsed TEA CO_2 lasers, where the temperature rise does not exceed 40 to 50°C [3]. However, when the gas temperature reaches 600°C, laser action will self-terminate. This is because of the increase of the upper level rate constant with increasing temperature, which is larger than that of the lower level [3].

From table 2.1, the addition of He is the real advantage in the deactivation of the (01^10) level and the lower laser levels while not affecting the (00^01) population. In the high-pressure

pulsed TEA CO_2 lasers, where thermal conductivity of the gas is not relevant, He has a favorable improvement of the discharge characteristics, especially those that operate near the region of instability. He, which has a first excited state level at 20.6-eV and an ionization potential of 24.5-eV, will not influence the discharge electron density n_e and average electron energy $\bar{u}_e$ where $\bar{u}_e \leq 5$ eV for TEA CO_2 lasers. However, the rate constant of k_{10} by He is still smaller than those of relaxation to (01^10) level (For example, 10^4-10^6 $torr^{-1}$ s^{-1} at 300K at pure CO_2). Therefore, the He partial pressure should be high for compensation (For example, 500 torr of He will give a relaxation rate of $4 \times 10^3 \times 500\ s^{-1} = 2 \times 10^6\ s^{-1}$).

The CO can also deactivate the v_2 level while H_2 and H_2O are used to reverse the dissociation of the CO_2 into CO and O_2 in sealed off systems (§2.7.1). However, H_2 and H_2O can decrease the laser output which eventually ceases to lase at high concentrations (§2.7.1). The addition of O_2 plays no significant collisional role but greatly influences the discharge stability (§2.3.3).

Table 2.1: Collisional relaxation rate constants of the CO_2 at 300 K in other gas (From Cherrington [70, p. 229], Tyte [71, p. 146]).

Relaxing gas	$v_3 \rightarrow v_2$ (k_{21}, $torr^{-1}$ s^{-1})	$v_2 \rightarrow$ ground (k_{10}, $torr^{-1}$ s^{-1})
CO_2 N_2	365 ± 15 110 ± 5	200 ± 10 ~40
He CO	≤ 85 193	$4 \pm 0.8 \times 10^3$ 4×10^3
H_2 H_2O	$4.1 \pm 0.3 \times 10^3$ $3.3 \pm 0.9 \times 10^4$	$7 \pm 3 \times 10^4$ 10^5-10^6
O_2	110 ± 5	~40

Note: the N_2^*-CO_2 collisional energy transfer rate constant is 1.9×10^4 $torr^{-1}$ s^{-1} at 300 K. N_2^* is referred to vibrationally excited N_2.

2.3 GLOW DISCHARGE FORMATION AND INSTABILITIES

The TEA CO_2 laser discharges usually work at high E/N and pd (product of pressure and laser channel gap) values and are usually created via the streamer breakdown mechanism [72, 73, 74, 75]. In this mechanism, a single-electron avalanche under the influence of high E/N and at high pd leads to rapid electron multiplication via secondary photoionization (Fig. 2.4) ahead of the avalanching streamer between the anode and the cathode. This usually leads to the development of a conducting filament and finally an arc channel bridging the anode and the cathode. The bridging process happens within a time as short as 10^{-9} s at high value of E/N [73]. This is the process by which most overvolt spark gap switches operate.

2.3.1 Effect of Preionization on Glow Discharge Formation

In order to suppress the above mentioned arc formation in the laser discharge, which is required to be homogeneous, a minimum preionization electron density (MPED) in the discharge volume has been found necessary. Fig. 2.4 shows a schematic diagrams of the initial and final charge distributions in a preionized breakdown. The local space charge field is smoothed out by the MPED. Calculation of MPED was first carried out by Palmer [74] in which ~10^4 electrons/cm^3 was predicted for a typical TEA CO_2 laser discharge. The model was further improved by Levatter and Lin [73]. In their model, they included (a) the effects of a finite voltage rise time on the depletion of free preionization electrons near the cathode during the preavalanche period and the effects on the subsequent development of the electron avalanche process, (b) the dependence of the first Townsend ionization coefficient α and the electron mobility μ on the applied E/N, and (c) the relation of a sizable error on the electron diffusion radius to the electron mean free path and the drift distance. The MPED for a finite voltage rise time of 1 to 100 ns in a 1-atm of 200:8:1-He:Xe:F_2 gas mixture is 10^6 to 10^4 cm^{-3}. The above

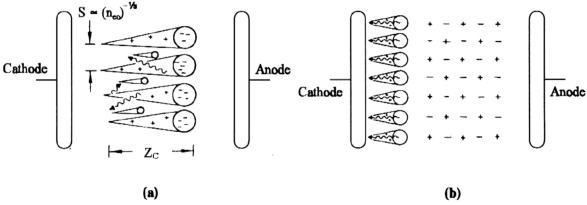

Fig. 2.4: Preionized breakdown initiated by multiple primary electron avalanches: (a) Initial, (b) final charge distributions (From Palmer [74]). S -- mean primary electrons (photoelectrons) distance; n_{eo} -- initial photoelectron density; Z_C -- critical avalanche track length. Wave-arrows indicate photons emitted from the primary avalanches and small avalanches in (a) represent secondary electron avalanches.

predicted MPED value was made with an assumption of preionization source strength constant up to the time of starting of the electron avalanche, giving a factor of 2 or 3 below the MPED value of undepleted region.

Gavirlov et al. [75] included an electron loss term in their calculations. The electron loss generally includes the three following processes: (a) diffusion of electrons from the discharge volume, which is negligible in the large volumes of TEA CO_2 lasers; (b) electron-positive ion recombination in which gas-phase recombination is generally too slow to be important at low preionization levels; and (c) an electron-neutral attachment, which is a dominant process in a gas mixture of more than 1% of CO_2 molecules by the dissociative electron attachment ($CO_2 + e \rightarrow CO + O^-$). In addition, the preionization electron density can also be reduced by oxygen through electron-neutral three-body attachment process ($e + O_2 + M \rightarrow O_2^- + M$, where M is any colliding particle [12]) in a close-cycle HRR TEA CO_2 laser [51]. The MPED predicted is an order or more higher than those estimated by Palmer [74]. By using inequality equations for

preconditioning requirements, i.e., the preionization electron density and the space charge field near the anode, they found that an increase of initial electron density would allow a wider range of applied electric field without increasing glow-to-arc transition.

2.3.2 Energy Input Period and Instabilities

In the energy input period, the discharge pulse length and the total input energy for an arc-free discharge depend on the ability of maintaining the plasma spatial homogeneity and temporal stability over the desired length of time [73]. However, if there is a small spatial and/or temporal amplitude fluctuations of the discharge parameters, such as local electric field intensity E_L, electron temperature T_e, electron density n_e, negative ion density n_n, positive ion density n_p, neutral particle density N, ionization α, and attachment β. The fluctuations of these parameters within the discharge cause different modes of instabilities to grow. These instabilities produce local current constriction within the medium resulting in highly nonuniform excitation and excessive local heating of the gas. Eventually, a highly ionized channel or arc is formed, causing the discharge voltage to rapidly collapse and generally, limiting the maximum discharge energy density. Several types of instabilities were found in TEA CO_2 laser discharges as described in the following.

(a) Ionization Instability

The ionization instability is often the most easy to occurr process in the conditions of a typical CO_2 laser discharge [16]. This ionization instability results from a temporal amplification of an imbalance between charged particle production and loss processes during a disturbance in the plasma properties. Negative ion formation was found to play an important role in causing this instability owing to decreasing electron density followed by increasing local electric field. However, the associative detachment of negative ions (CO_3^- and O^-) by CO and reduction of O_2

concentration could suppress the onset of ionization instability. The former occurs mainly via $CO_3^- + CO \rightarrow 2CO_2 + e$ and $O^- + CO \rightarrow CO_2 + e$ reactions [12] whereas the latter case is via catalytic process [65, 12].

(b) Attachment Instability

Douglas-Hamilton and Mani [17] found that the electron-neutral dissociative attachment rate increases strongly with discharge electric field. When an electron attachment process occurs, the electron density is reduced. Consequently, the local electric field is increased. This will further increase the attachment rate. An instability then occurs which is almost the inverse of the ionization instability due to increasing electric field followed by decreasing electron density. Under certain conditions, this attachment instability may trigger localized ionization instabilities due to increasing local electric field.

(c) Thermal Instability

The thermal instability is a relatively slow process. It is more likely to happen on the cathode surface due to the cathode fall. The high electric field distortion at the cathode surface will lead to localized region of high current density via localized ionization. This localized current heating will lead to the increasing cathode emission process and increasing E/N value. Therefore, the electron density is further increased locally. If this process is sufficiently rapid, the formation of arc channel can occur.

Fig. 2.5 shows a typical transition from a glow discharge to an arc discharge. The different mode of instabilities may approximately happen during the transition of the first glow phase to the second glow phase. The arc formation may happen either during the discharge or the afterglow. In addition, the resultant nonuniform distributions of refractive index within the inhomogeneously excited medium (second glow phase) make the formation of high opticalquality laser beam difficult.

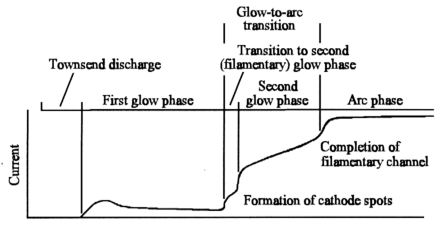

Fig. 2.5: Transition from a glow discharge to an arc discharge (From Yokoyama et al. [76]).

Sakai et al. [10] used a high-speed-camera operating on a streak mode to study the spatiotemporal development of a gas discharge. They also used time-resolved streak and time-integrated photographic techniques as well as current- and voltage-oscillographic techniques to study this glow-to-arc transition. In that study, the instability appears as a bright spot at the cathode in the middle of the self-sustained uniform glow stage (the glow duration t_g is about 0.5 μs) and continue for about 450 ns which then propagates in the anode direction (anode-directed) with a speed of about 0.6 cm/μs in 1-atm of 1:1:8-CO_2:N_2:He gas mixture, keeping the shape of a bright spot until it reaches the middle of the gap. After that it develops rapidly into two constricted bright filaments, i.e., the anode-directed and the cathode-directed with speeds of 9.0 and 1.2 cm/μs respectively. Finally, a bright highly conductive channel is formed as a result of the arrival of both-directed filaments at the electrode surfaces. This glow-to-arc transition takes a duration of about 1 μs.

The circuit parameter study revealed that a faster rise time of the applied voltage to the main gap can prevent the arc formation, though the bright spot or filament still appears on the anode and cathode surfaces. Furthermore, this fast voltage rise time circuit can make a longer

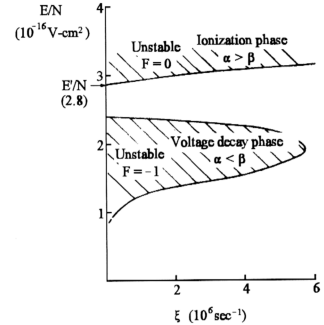

Fig. 2.6: Stability diagram for a discharge in a 1:1:8-CO_2:N_2:He mixture at atmospheric pressure. E'/N is the value at steady-state operation. ξ and F are parameters in the instability condition equation derived by Dyer and James. **α** and **β** are the ionization and attachment coefficients (From Dyer and Tait [9]).

glow duration before arc formation. The cathode surface condition can also affect the glow duration t_g and also the peak glow current. A decrease in t_g and t_a (arc formation time) were also observed after arc induced damage appears on the surface of the cathode.

Dyer and James [9] have shown that arc formation at high energy densities generally occurs in one of two distinct regions in the TEA CO_2 laser discharge cycle, i.e., near to the peak of the discharge current pulse on the falling edge and in the 'tail' of the current pulse. Fig. 2.6 shows the two unstable regions. The instability condition equation used to generate this figure is based on the ionization-attachment rate equations and finding the conditions when perturbations in the electron density grow in time with neglecting the electron temperature

dependence of electron-ion recombination coefficient. The parameter ξ is defined as:

$$\xi = [\ (2\gamma + \kappa) + (\gamma + 2\kappa)\ n_n / n_e\ ]\ n_e \qquad (2.5)$$

where γ = electron-ion recombination coefficient, κ = ion-ion recombination coefficient, and n_n = negative ion density. In steady-state condition (E'/N = E/N), the electron production through ionization is balanced with electron losses through electron-neutral attachment and electron-ion recombination. However, in a typical TEA CO_2 laser discharge, recombination process is much slower than the attachment process. The upper region (F = 0) shows that initial perturbations in electron density are maintained through the ionization phase of the discharge. Since this region has values of E > E', $\alpha < \beta$, ionization dominates attachment. The growth rate of ionization instabilities at atmospheric pressure is typically in the range of 10^6-10^7 s^{-1}, which is sufficiently large for the instabilities to be significant during the discharge lifetime. In the lower region (F = - 1), the authors predicted that the low field instability can be stabilized by recombination if ξ is about greater than 6×10^6 s^{-1}. But attachment dominates recombination during this voltage decay period. This region is E < E', so $\alpha < \beta$ and attachment dominates ionization. Arc formation in this region is strongly dependent on the circuit parameters. This simple stability analysis neglected the variations in the instability growth rate through the discharge cycle, the stabilizing influence of detachment, and, on relatively long time scales, gas heating effects as mentioned by the authors.

2.4 THE E/N AND EXCITATION EFFICIENCY

Besides the creation of a homogeneous discharge, an optimum E/N (the ratio of interelectrode electric field to neutral particle density) value largely governs the electron

excitation of the $CO_2(00^01)$ level and $N_2(v = 1\text{-}8)$ levels. The electron excitation cross sections for $CO_2(00^01)$ and $N_2(v = 1\text{-}8)$ depend on the electron energies, as mentioned in §2.2.2. Furthermore, the electron energy distribution function f(u) is sensitive to the E/N for a given gas mixture [56]. The dependency of f(u) on gas mixture for a given E/N changes slightly at the electron energies of interest (few eV). For gas mixture of 1:1:8-CO_2:N_2:He, the optimum E/N is 1.2×10^{-16} Vcm^2 with 74% excitation efficiency to $CO_2(00^01)$ level and $N_2(v = 1\text{-}8)$ levels [56]. For gas mixture of 8:8:84-CO_2:N_2:He (premixed industrial-grade mixture, Laser 88), the optimum E/N is slightly lower than that of 1:1:8 [77].

The quasisteady-state E/N value of a self-sustained discharge of 1:1:8 is $\sim 2.7 \times 10^{-16}$ Vcm^2 [78], which is larger than the optimum E/N value. For a given gas mixture, the quasisteady-state E/N is independent of the usual operating ranges of discharge current density, total pressure, and electrode spacing [78]. However, the existence of small amount (<1%) of attaching species (e.g., CO_2, H_2O, and O_2) can shift the quasisteady-state E/N to higher value [78]. This may reduce the laser efficiency as described by Howells and Cridland [79].

Analysis of E/N values was done by Cridland and Howells [52] by calculation of energy deposited into the discharge at discrete intervals of E/N from the measured voltage and current waveforms. They found that the single-capacitor discharge (SCD) circuit is the most efficient as compared to other circuit configurations. This is because the SCD circuit deposits the largest proportion of its storage energy at low range of E/N values, which are closer to the optimum E/N value.

By using an inductor in the excitation circuit [80], e.g., between the storage capacitor and laser head, it can reduce the operating E/N value during the current pulse if the discharge uniformity is unaffected. This is mainly caused by the voltage drop in the inductor during the current pulse and the peak current occurs at lower discharge voltage across the laser channel due

to slower current rise time. As a result, the electrical-to-optical conversion efficiency can be increased. It was found by Howells and Cridland [80] that the ratio of gain-switched spike to tail energy of the laser pulse was decreased with the increase of the inductance, the N_2 tail energy area increased. However, prolonging the duration of the current pulse can lead to discharge instabilities and arcing.

2.5 POPULATION SATURATION IN TEA CO_2 LASER

In §2.4, the excitation efficiency, 50-80% for typical values of operating E/N, did not include the deactivation of vibrationally excited N_2 and CO_2 molecules by electron superelastic collision [81, 82] in which vibrational energies are lost into the plasma electron as well as the molecular collisional deactivation or relaxation processes of N_2 and CO_2 (§2.2.3). Therefore, the predicted electrical-to-optical efficiency (yield efficiency) is higher than the actual value. For TEA CO_2 oscillator, the laser action is inhibited during the current pulse by the large population excited to the $CO_2(\nu_1, \nu_2)$ mode, which contains the lower laser levels. This population relaxes on a time scale of approximately 1 μs after the end of the excitation pulse, only then will oscillation occur. Under these circumstances, superelastic losses during the current pulse should limit the available vibrational energy for subsequent conversion to laser radiation.

Fig. 2.7 shows the predicted total energy density store (ε_S) in N_2 and $CO_2(\nu_3)$ vibrations as a function of input energy density ε_{in}, which illustrates the effects of electron superelastic losses (saturation of ε_S with increasing ε_{in}) and molecular collisional relaxation losses (decreasing in ε_S with time after the excitation pulse). Note that, ε_S at the end of excitation pulse is the maximum whereas the peak gain corresponds to the maximum population inversion. At very low ε_{in}, the energy storage $\eta_S = \varepsilon_S/\varepsilon_{in}$ approaches the assumed excitation efficiency $\eta_{ex} = 60\%$. However, at all higher input energy densities, the η_S is degraded by superelastic losses as the

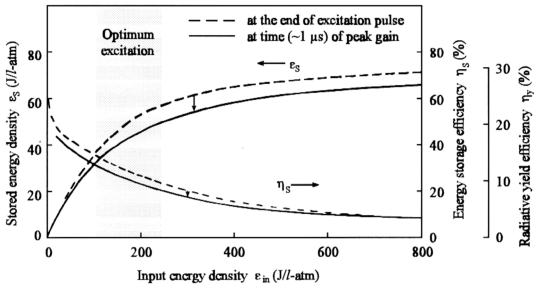

Fig. 2.7: Predicted energy storage density of N_2 and $CO_2(v_3)$ vibrations and storage efficiency $\eta_S = \varepsilon_S/\varepsilon_{in}$ for 100-ns pulse conditions (square current pulse with constant n_e and effective E/N), which were assumed by Smith and Mellis, at 760 torr of 13:9:78-CO_2:N_2:He with an assumption of 60% of $N_2 + CO_2(v_3)$ pumping efficiency η_{ex} (From Smith and Mellis [82]).

product of excited population and discharge electron density n_e becomes large. Therefore, η_S is a function of both ε_{in} and n_e. In the normal operating region of ε_{in} = 100-200 J//-atm, the superelastic losses are still effective. The product $\eta_S\varepsilon_S$ is a useful figure of merit in describing the efficiency of the stored system energy. This is a maximum in the region indicated (ε_{in} ~ 150 J//-atm), where the predicted η_S is 20 to 30%, and the resultant radiative yield efficiency η_y = 8-12% ($\eta_y = \eta_S\eta_q$ where η_q ~ 41% is the quantum efficiency of the CO_2 transition). Note that if laser action occurs during the current pulse, the practical yield efficiency η_y (or electrical-to-optical) may be higher than that of the predicted value.

2.6 FREQUENCY LIMITATIONS IN HRR TEA CO_2 LASER

The frequency limitation in the HRR TEA CO_2 laser was studied by Dzakowic and Wutzke [11] and Baranov et al. [83, 84]. Repetitively pulsed, stable and arc-free glow discharges

can be achieved when the gas discharge products are removed from the interelectrode region during the time interval between current pulses. For low repetition rates, e.g. 20 pps (pulse per second), the charged particles are removed through recombination processes between current pulses, and stable glow discharges are formed. The laser pulse energies are reduced by the increase of gas temperature and thermal diffusion is usually the dominant cooling process. At a higher repetition rate, in the range of several 100 to 1000 pps, the discharge products are removed by convection, normally the gas flow is in the direction transverse to the discharge current.

2.6.1 General HRR Characteristics

Typically, the operation frequency of HRR TEA CO_2 laser may be increased until the pulse glow discharge becomes unstable resulting in arc formation. The onset of arcing imposes the limitation on the maximum input power into the glow discharge, and hence limiting the maximum output power of the laser (Fig. 2.8).

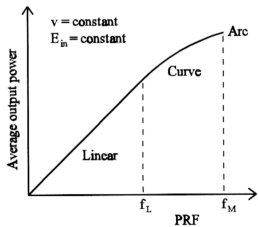

Fig. 2.8: Typical dependency of average output power to PRF of a HRR TEA CO_2 laser. v is the interelectrode gas velocity, E_{in} the input energy per pulse, and f_L and f_M the maximum frequencies of constant average output energy per pulse and of arc-free glow discharges. Assuming, other parameters and conditions are unchanged along the increase of PRF.

Experiments have found that the minimum time between arc-free pulses ($1/f_M$) falls within 2-5 times [11] of the transverse time for gas-flow across the laser channel. Given the discharge width (w) and gas velocity (v), a clearing ratio CR is defined as follows [11]:

$$CR = (1/f_M) / (w/v) \tag{2.6}$$

The CR values are » 1 for the linear region in Fig. 2.8, and ~ 1 for the curved region.

Fig. 2.9 shows the maximum PRF, f_M, for the arc-free discharge as a function of gas velocity v, as reported by Dzakowic and Wutzke [11]. From this figure, f_M is linearly dependent on gas velocity.

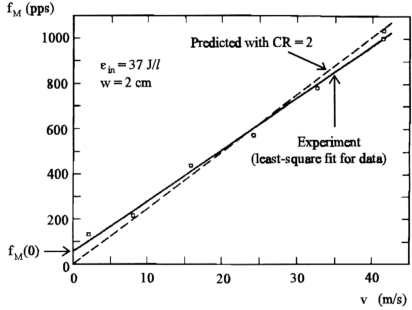

Fig. 2.9: Maximum PRF for arc-free discharge f_M vs gas velocity v. ε_{in} is the input energy density per pulse and $f_M(0)$ the maximum PRF without gas flow. The storage capacitance and its voltage are constants and the laser is operated at 510 torr of 50:50:400:10-CO_2:N_2:He:H_2 (From Dzakowic and Wutzke [11]).

The value f_M also depends on the input energy density ε_{in} as shown in Fig. 2.10. For a given ε_{in}, f_M was independent of capacitance from 9 to 36 nF [11]. From this figure, the maximum average input power density is ~60 kW/l at ~100 J/l and ~600 Hz. It was found that this maximum average input power density decreases linearly with the flow velocity [11]. Generally, the maximum attainable average output power has been reported to be 5-10 times less than the theoretical limit, i.e. $P_0 = E_0 \times (v/w)$, where E_0 is the maximum output energy per pulse in single-pulse mode [83].

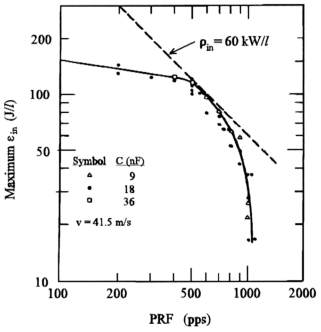

Fig. 2.10: Maximum input energy density per pulse ε_{in} vs PRF. C is the storage capacitance and ρ_{in} the average input power density. The operating pressure and gas mixture are the same as in Fig. 2.9 (From Dzakowic and Wutzke [11]).

For a given flow velocity of 41.5 m/s as in the case of Fig. 2.10, the clearing ratio ($\propto 1/f_M$) increases with input energy density ε_{in} if we take f_M as a function of ε_{in} from Fig. 2.10. There are three main factors to explain the observed clearing ratios, which limit the maximum PRF or affect the average output power, namely the (1) boundary layers on the electrodes, (2) adiabatic

(isentropic) expansion and heat conduction (thermal diffusion) of a heated gas, and (3) shock waves and acoustic waves. The first two limit the maximum PRF whereas the third one affects the discharge stability.

Fig. 2.11 shows the schematic diagram of the discharge chamber with the three components that influence the discharge.

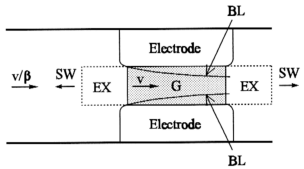

Fig. 2.11: Schematic diagram of discharge chamber. G is the glow discharge region, BL the boundary layers on electrodes, EX the expanding gas regions, SW the shock waves, v the interelectrode gas velocity, and **β** the ratio of upstream to interelectrode flow cross-sectional areas (From Dzakowic and Wutzke [11], Baronov et al. [83]).

2.6.2 Effect of Boundary Layers

Insufficient removal of the discharge gas from the boundary layer, where the velocity changes from zero on the electrode surface to a maximum (smaller than that outside boundary layer) on the layer boundary, is one possible mechanism limiting the PRF. This hydrodynamic boundary layer has the minimum thickness at the upstream edge and maximum thickness at the downstream edge of the electrode (Fig. 2.11). Holographic interferometry showed this effect in a 100-torr N_2 gas flow with a delay of 9 ms after electrical pulse [84]. Gas clearing in this layer is dominated by diffusion processes; fresh gases diffuse into and discharge gases diffuse out from the boundary layer. The resultant inhomogeneity of the gas density along the boundary layer means inhomogeneity of E/N, subsequently, the output energy per pulse is reduced before arcing

occurs. For a laminar boundary layer velocity distribution, the clearing ratio CR has been estimated from a minimum value of $\sqrt{3}$ with the consideration of the maximum diffusion time to the layer boundary [11]. When the nature of flow in the boundary layer changes from laminar to turbulence (varying direction) and when the gas stream velocity as well as the Reynolds number are high (Reynolds number increases, resulting decrease of boundary layer thickness), the effect of the boundary layer on PRF is reduced considerably [83].

2.6.3 Effects of Adiabatic Expansion and Heat Conduction

The sudden heating of the gas in the glow discharge will produce pressure waves (shock waves) and rapid expansion of the heated gas or discharge products under adiabatic (isentropic) process. The expansion of this discharge products due to gas heating will be called 'puffing' [11]. This rapid expansion (Baranov et al. observed that the expansion grows linearly [84]) will be slowed down when the pressure inside the heated gas is equal to the surrounding pressure (~100μs [11, 84]), and then the thermal diffusion will take place to give a slower expansion stage (~1-2 ms [84]). Baranov et al. [84] used shadow or Schlieren photography and holographic interferometry techniques to show two stages of the heated gas expansion, i.e., the adiabatic expansion and thermal diffusion. In the first rapid stage, the contact surface (boundary between heated and unheated gas) moves out (puffs) into the relative low-pressure surrounding region with a speed of slightly less than sonic. In the second slower stage, diffusion begins with a turbulence type since its velocity is much larger than the gas flow velocity v ($v \ll$ sonic), which then becomes of the molecular type when diffusion velocity is less than or equal to v. So the heated gas is considered to be stationary during the quick expansion stage and is an expanding moving slug during the diffusion stage.

The expansion of this heated gas depends on the input energy density e_{in}. The ratio of the

expanded discharge width w' to the discharge width w immediately after discharge, ER, due to adiabatic expansion can be derived. By using the equations of state and energy for ideal gas heating at constant density followed by adiabatic expansion of the gas to the initial pressure [11, 48, 84], ER is defined as

$$ER = w'/w \tag{2.7}$$

$$ER_{ad} = (T_f / T_i)^{1/\gamma} \tag{2.8}$$

$$ER_{ad} = (1 + \varepsilon)^{1/\gamma} \tag{2.9}$$

The term $\varepsilon = (1 - \eta)\varepsilon_{in} / \varepsilon_{int}$ is the normalized input energy density as heat to the internal energy density ε_{int} of the gas mixture which can be expressed as $\varepsilon_{int} = \rho c_v T_i$ at operating pressure p [11]. $\gamma = c_p/c_v$ is the ratio of specific heat capacities of the gas mixture which is taken to be approximate 1.5 [11]. T_i and T_f ($T_f > T_i$) the initial and final temperature in the discharge heated gas slug, ρ the density of unheated gas mixture at pressure p, and η the electrical-to-optical energy conversion efficiency of the laser. The clearing ratio is then [11, 48]

$$CR = 1 + \tfrac{1}{2}\beta(ER - 1) \tag{2.10}$$

where β is the ratio of upstream to interelectrode flow cross-sectional areas.

For an energy input of 300 J/l-atm, the adiabatic expansion is $ER_{ad} \sim 1.4$-2.0 range. This will give a limit of CR ~ 1.2-1.5, taking $\beta = 1$ [84]. Considering both adiabatic expansion and diffusion, CR ~ 1.7 [84]. Fig. 2.12 shows the comparison of predicted and measured clearing ratios which were influenced by the input energy density ε [11]. At low input energies ($\varepsilon < 0.3$), the clearing ratio is dominated by boundary layer diffusion which has a value of $\sqrt{3}$ for laminar

boundary layers. At high input energies ($\varepsilon > 1.3$), the single-pulse glow stability limit is encountered and the CR tends to infinity and arcing occurs frequently. The maximum ε value is system dependent and can only be found experimentally. For this system, this value is about 1.3 as shown in Fig. 2.12. The gas puffing limit is determined by the adiabatic expansion equation without considering the diffusion expansion. From this figure, the maximum average input power density (60 kW// in Fig. 2.10) is limited by the gas puffing.

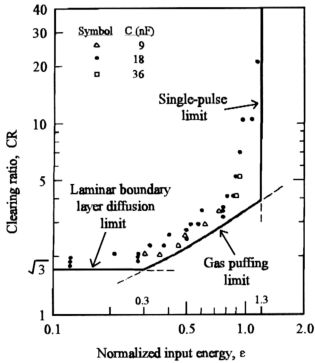

Fig. 2.12: Comparison of predicted and observed clearing ratios. The normalized input energy density ε is defined as in text. The operating pressure and gas mixture are same as Fig. 2.8 and $\beta = 7.35$ and $\gamma = 1.5$. Adiabatic expansion equation is used for predicting gas puffing limit (From Dzakowic and Wutzke [11]).

It is noted that the adiabatic expansion directions may not be in the direction of gas flow, it may widen in the discharge current direction when the heated gas expands beyond the interelectrode region. Furthermore, the nature of flow, laminar or turbulence, in the discharge region could also affect the discharge gas diffusion, in which a turbulent flow could lead to an

increase in the required CR [83].

2.6.4 Effects of Shock Waves and Acoustic Waves

Shock waves are formed at the edges of the glow region because the inertia of the gas allows a constant density pressure rise during the rapid uniform heat input. These shock waves separate from the contact surfaces and move away from the heated region with a speed greater than sonic velocity. Baranov et al. [83, 84] used holographic interferometric methods to show that gasdynamic perturbation appeared in the discharge gap. It shows perturbation of the gas traveling in both directions from the discharge and the shock waves generated at the electrodes (electrode shock waves) because of the higher rate of energy release in the electrode layers. The intensity of gasdynamic disturbances depends upon energy input density, energy release time, and nature of the gas. The shock wave dissipates its energy as heat in the gas where it passes through. However, numerical estimates show that, for typical discharge parameters, the heating of the gas due to energy dissipation in the wavefront is quite negligible [83].

Besides the shock waves, there is also a number of reflected rarefaction (expansion) and compression waves. Their general feature is a reduction in the wave amplitude, slowing down of the energy dissipation, and increase in the wavelength, to eventually becoming an acoustic wave. Laser channel is also treated as an acoustic cavity. Resonant excitation (acoustic vibrations are absorbed and radiated by the gas channel) of the natural frequencies of this acoustic cavity occurs during the repetitively pulsed energy input. This resonant excitation is possible during standing acoustic wave formation. The natural vibrations being resonantly excited in the channel can induce gas density inhomogeneities in the interelectrode gap and cause arcing because these inhomogeneities cause the change of E/N along the discharge electrode. In subsonic gas flow, acoustic disturbances resulting from heat evolution in the discharge propagate both downstream

and upstream from the flow. It was experimentally found that, in addition to these acoustic waves in the laser channel, waves can form transversely to the gas flow if the side walls of the channel reflect the sound. In a certain range of parameters for the transverse waves, where a transverse standing acoustic wave is formed, the resonant excitation induces discharge luminosity modulation. This phenomenon has been observed by Baranov et al [84] where the maximum output power reduction occurred at frequencies ~350 pps and ~600 pps and minimum output power reduction at ~500 pps and ~650 pps with the reduction of laser output power by gas perturbation starting to occur at ~250 pps.

Attenuation (e.g., by baffle grids) of these waves at subsonic flow velocity does not depend on the flow velocity and is determined only by the geometry of the discharge chamber and gasdynamic channel. If the gas density disturbance from the shock wave induced by the previous discharge has not damped before the succeeding discharge, it can cause a discharge nonuniformity. The high sensitivity of the pulse discharge to the density disturbances leads to an instability of a new type, i.e. thermal-acoustic instabilities [84].

2.7 GAS DEGRADATION IN HRR TEA CO_2 LASER

The degradation of laser gases is detrimental for HRR TEA CO_2 laser operation. Gas mixture degrades by decomposition of active molecules (CO_2 and N_2) and formation of contaminants or impurities (CO, O_2, O_3, N_2O, NO_2, and NO), which make laser operation unstable. Various species of molecules, ions, and cluster molecules and ions (e.g. O^-, O_2^-, CO_3^-, CO_4^-) are formed during and after the electrical discharge. Therefore, the CO_2 content and excitation efficiency are decreased. The latter is caused by O_2, which can lead to the increasing E/N value and discharge instability. Hence, the laser output efficiency is reduced.

2.7.1 Dissociation and Reformation Reactions

A CO_2 molecule can be dissociated by two electron-collision initiated reactions, as shown in equations (2.11) and (2.12). The dissociation rate of the first reaction is several tens of times faster than that of the second reaction. A N_2 molecule is dissociated into (N + N) by electron-collision. This N_2 dissociation rate is 1-3 orders of magnitude slower than that of the CO_2 at typical E/N = 2.0-4.0 × 10^{-16} Vcm^2 [13].

$$e + CO_2 \rightarrow CO + O + e \quad \text{(Neutral dissociation reaction)} \tag{2.11}$$

$$e + CO_2 \rightarrow CO + O^- \quad \text{(Dissociative attachment reaction)} \tag{2.12}$$

$$e + N_2 \rightarrow N + N + e \quad \text{(Neutral dissociation reaction)} \tag{2.13}$$

The reformation reactions of CO_2 and N_2 are mainly the neutral three-body reactions [13]:

$$O + CO + M \rightarrow M + CO_2 \tag{2.14}$$

$$N + N + M \rightarrow M + N_2 \tag{2.15}$$

where M is the colliding particle. The N_2 reformation reaction is more than 10^3 times faster than the CO_2 reformation reaction at room temperature and at an atmospheric pressure. Owing to the great difference in the dissociation and reformation rates between CO_2 and N_2, the fractional decomposition (the ratio of the total net decomposed number to the initial existing number) of N_2 is much smaller than that of CO_2, which is 0.18% for N_2 and 75% for CO_2 after 1.7 × 10^5 pulses at ~180 J/l and 15:15:70-CO_2:N_2:He [13]. Therefore, the concentrations of the by-products of N_2 (N_2O and NO_2 dominantly) are much smaller than those of CO_2 (CO, O_2, and O_3). The nitrogen oxides are identified as minor products with negligible concentrations as compared to

CO and O_2 [15].

The decomposition of CO_2 molecules can be reduced by using catalysts such as CO, H_2, and H_2O. These gaseous catalysts increase the following reaction rates [13, 14]:

$$CO + O + M \rightarrow M + CO_2 \quad \text{(Neutral three-body reaction)} \quad (2.16)$$

$$OH + CO \rightarrow H + CO_2 \quad \text{(Neutral two-body reaction)} \quad (2.17)$$

$$e + H_2O \rightarrow H^- + OH \quad \text{(Dissociative attachment reaction)} \quad (2.18)$$

The CO_2 formation via reaction (2.16) is several tens of times slower than those of H_2 or H_2O.

Hokazono et al. [13] calculated that, for a given gas mixture of 15:15:70-CO_2:N_2:He and input energy density of ~180J/*l*, the fractional CO_2 decomposition at equilibrium (after 10^5 pulses) steeply decreased from 93% to 51% when the H_2O concentration was increased from 0 to 100 ppm (part per million). Further increase of H_2O content (> 100 ppm) did not decrease the equilibrium CO_2 decomposition level significantly (at 1000 ppm H_2O, CO_2 decomposed ~47%). Experiments showed that 20% to 40% of CO_2 is decomposed at around input energy density of 100 J/*l* in different gas mixtures. This is because gas mixture in laser chamber normally contains a trace of water vapour from several tens ppm to several hundreds ppm, which come from outgassing of the laser chamber wall and other gas cylinders or pipings exposed to the atmosphere or had originally existed in the technical grade laser gas mixture as an impurity. Calculations showed that 30% of CO_2 is decomposed with addition of 100-ppm H_2O at 100 J/*l* and 15:15:70-CO_2:N_2:He. For a given H_2O concentration, the equilibrium CO_2 decomposition level increased almost in proportion to the square root of the input energy density.

The H_2O is an electronegative (attaching) species resulting in an increase of E/N and a decrease of discharge stability and is very effective in the relaxation of $CO_2(v_3)$ (§2.2.3). Both

effects can degrade the laser performance when its concentration is too high (probably <1%) in the gas mixture. H_2 can also give some negative effects on the laser performances; such as its reaction with CO_2 to produce H_2O, and thereby subsequently, reduces the CO_2 concentration. The addition of H_2O, H_2, and/or CO into the CO_2:N_2:He mixture can lead to decrease of the laser output energy or average power but produce a longer lifetime with a reduction of O_2 concentration level tolerance due to the high electronegativity of the additives [55]. It is because these additives (H_2O and H_2) can highly depopulate the $CO_2(v_3)$ level, which also compete with the stimulated emission (§2.2.3). Quenching of laser output may occur when H_2 concentration reaches ~15% in 1:1:3-CO_2:N_2:He mixture [46] and when H_2O reaches <1%. In practice, the H_2 concentration ranges from 0.1 to 7% in various gas mixture [12, 41, 42, 43, 46, 85] and the CO concentration from 0.2 to 15% [12, 44, 51, 55, 65, 85], which depends on the circuit scheme.

Solid state catalysts such as Pt(Pd)/SnO_2, Pd(Pd)/Al_2O_3, and Pt/Fecralloy [86] can be used to reform CO_2 through the reaction

$$CO + O + S \rightarrow S + CO_2 \tag{2.19}$$

where S denotes the catalyst surface [13].

2.7.2 Effects of Gas Mixture Degradation

The dissociation of gas molecules in CO_2 laser mixture of CO_2:N_2:He by electrical discharge produce various stable species and metastable or decaying species. The stable species are accumulated in the closed-cycle laser chamber resulting in the ratio of CO:O_2 of 2:1 [15] after the gas discharge is switched off for a long enough time for O_3 to decay to O_2 and the ratio of O_3:O_2 is 0.23:1 [13] during the laser operation. As mentioned previously, the accumulated

nitrogen oxide (N_2O and NO_2) concentrations are far smaller than O_3, and can be negligible. The NO was also observed at very low level since NO can be oxidized to form NO_2. Due to these accumulated species and the original molecules CO_2 and N_2, a vast number of metastable species are formed during and after the glow discharge. The negative ions, which are quickly formed in a time scale of nanosecond [12], are mainly O^-, O_2^-, CO_3^-, and CO_4^- [12, 87]. The CO_3^- is the dominant negative ion when fresh gas mixture discharge is performed. However, when O_2 level is increased, the CO_4^- dominates.

At least four types of effects can occur due to the accumulated species (CO, O_2 and O_3) on the laser performance:

(a) negative ions formation, which can cause discharge instabilities (§2.3.2) by dissociative attachment reaction [13];

(b) UV absorption, where O_3 and O_2 highly absorb UV radiation. The short UV absorption depth can cause the spatial inhomogeneity of the preionization, especially in the wide-aperture TEA CO_2 laser. A 1.5% of CO_2 decomposition will lead to a decrease of the UV absorption depth by 30% [13];

(c) preionization electron attachment, where O_2 is an electronegative species. The photoelectrons, which are created by the preionization process, rapidly attach to the O_2 molecule by the three-body attachment process. Consequently, the effectiveness of the preionzation is decreased [51], and

(d) increase of E/N, where the attaching species can increase the electron loss by attachment and a new electron gain-loss equilibrium need to be achieved by increasing E/N (§2.4).

It has been reported that 1% of O_2 concentration could reduce the laser output energy by 50% [15].

2.7.3 Electrical Parameters Effects on Gas Mixture Degradation

The discharge initiated decomposition of CO_2 molecules is almost proportional to the electrical energy deposition in the laser gas mixture [13, 14, 15]. This relation is true only when E/N values are maintained to be the same for different input energies. Smith and Austin [88] found that the dissociation rate of CO_2 increases with E/N. This E/N effect on CO_2 dissociation was also observed by Matsumoto et al. [54] for TEA CO_2 laser. Other parameters (such as circuit inductance [80]), which affect the E/N value, will also affect the CO_2 dissociation.

Besides the main discharge, the preionizer discharge can also contribute to the CO_2 dissociation but is $\sim 10^3$ times smaller than that by the main discharge. The surface spark array dissociates CO_2 more than that by the pin spark array [54] which in turn is more than the trigger wire [85]. In the first case, it was probably due to the smaller discharge resistance and less energy dissipation in the pin spark array than the surface spark array while the second case was due to the difference between the glow discharge (trigger wire) and arc discharge. Therefore, the semiconductor [29, 85] or corona [46] preionizer, in which the preionizing discharge contains no arcs, was used for sealed-off mini-TEA CO_2 lasers.